Instrument Science Report STIS 2018-06

Impacts of focus on aspects of STIS UV Spectroscopy

Allyssa Riley[1], TalaWanda Monroe[1], & Sean Lockwood[1]

[1] Space Telescope Science Institute, Baltimore, MD

November 7, 2018

ABSTRACT

The STIS Instrument focus has been drifting more and more positive over time since the Optical Telescope Assembly (OTA) was shifted in 2011. Unfortunately, the STIS best focus was found to be at more negative focus values relative to HST observatory focus. However, this slight upward trend in focus is still smaller than the orbital variation in focus that is seen due to the thermal evolution of the telescope. Both the upward trend and the change in focus due to the orbital variation come into play and this is why sometimes the absolute focus is closer to STIS best focus than at other times. When the absolute focus is not close to STIS best focus, some spectroscopic data has been observed to have larger FWHM values and more spatially dispersed profiles, causing flux anomalies in data. This document discusses these flux anomalies and outlines analysis done to determine whether the Enclosed Energy (EE) tables contained in the HST Exposure Time Calculator (ETC) or the Photometric Conversion Table (PCTAB) have changed. We also discuss what the user community might expect to see in their data due to the changing focus of STIS.

Contents

Operated by the Association of Universities for Research in Astronomy, Inc., for the National Aeronautics and Space Administration.

1. Introduction

The Space Telescope Imaging Spectrograph (STIS) uses three detectors, including two Multi-Anode Microchannel Arrays (MAMAs) that operate in the NUV and FUV. The MAMAs are used in spectroscopic observations and are highly sensitive. Too much light can severely damage MAMA detectors, so the STIS team must ensure the safety of these detectors for every proposal asking for MAMA time. Because of this, all Principle Investigators (PIs) proposing to use the MAMAs are required to prove to the STIS team that their observations, given the selected grating, aperture, and exposure time, will not damage the MAMAs, and the results of the Exposure Time Calculator (ETC) is their proof.

The HST ETC uses tables of Enclosed Energies (EE) to calculate reasonable exposure times and expected signal-to-noise ratios for the parameters given. The EE tables used by the ETC include percent fluxes expected within various extraction heights ranging from 1 pixel to the default extraction heights for the first order MAMA modes of 11 pixels, all the way out to an extraction height of 600 pixels for each available grating (see Tables 4-7 for the current EE tables in the ETC). Besides helping in bright object protection and estimating performance through the ETC, the EE tables are also used in the Photometric Conversion Tables (PCTABs), which ensure an accurate absolute flux in the final flux calibrated spectra. The PCTAB provides the throughput at each extraction box size, with the throughput vector at the default extraction size (11 pixels for the first order MAMA modes) defined as unity.

Despite the importance of the EE tables, they have not been updated since 1998 and the PCTAB has not been updated since 1998 and 2014 for the M-modes and L-modes, respectively. The STIS team has recently found evidence that the STIS focus

relative to observatory focus has been drifting in the positive direction since 2011, when observatory focus was shifted to track the Optical Telescope Assembly shrinkage rate of WFC3 and ACS. Because STIS was following a different trend than those two instruments, this adjustment has caused STIS focus to drift by $\sim$1.25 microns per year, but has recently started to slow (Proffitt, et al 2017). Because STIS best focus is at more negative values, this drifting is responsible for a loss in throughput by up to 25-60% in small apertures, depending on the specific breathing and focus evolution of the particular program (Proffitt, et al 2017). It is important to note that there is also orbital variation in focus due to the telescope's thermal evolution. This orbital variation can be constructive or destructive with the focus offset. Thus, sometimes the absolute focus is close to STIS best focus and sometimes it is more positive. If it is more positive, this misfocus spreads out the signal of the target, so the spectra are not as spatially compact as when the instrument is in focus, resulting in overly-large full width at half maxima (FWHMs).

In 2017, these unexpectedly large FWHMs were found in a subset of NUV-MAMA observations. Usually, the FWHMs of the NUV-MAMA data are 3-4 pixels, but these datasets showed FWHMs of 5-6 pixels, as shown in Figure 1. We suspected that this variation in the FWHMs corresponded to a change in focus. When the spectrum is out of focus, some of the source flux may lie outside of the extraction box or the slit, in the case of small apertures. An example of what this might look like in the 2-dimensional spectrum is shown in Figure 2.

2. Qualitative Impacts to More Positive Focus

Because the STIS focus is not constant, it is important for users to know how a changing focus can affect science data, and how to identify whether their observations were taken when the focus was very positive or negative relative to HST observatory focus.

2.1 Negative and Positive Focus

We show two examples of negative and positive focus for the NUV-MAMA from GO 13145 and 13548. Both of these were taken with the 52X2 aperture, and the G140L grating at central wavelength 1425 Å. We plotted the spatial profiles, then took the focus model values from the 2016 annual summary files and interpolated between data points to the middle of the observation. Using this, we were able to demonstrate the correlation between FWHM and focus value at the middle of the observation. An example of this can be seen in Figure 1.

Figures 1 and 2 help confirm the finding by Proffitt, et al 2017 that the STIS instrument is most in focus at negative focus values. The left panel of Figure 2 shows the dataset oc4kl1010, which was observed at a focus of -6.27 microns and, as a result, has a small FWHM of 3.6 pixels. Compared to the left panel however, the spectrum to the right is much more diffuse. The right panel displays the dataset ocetl2010 which has a

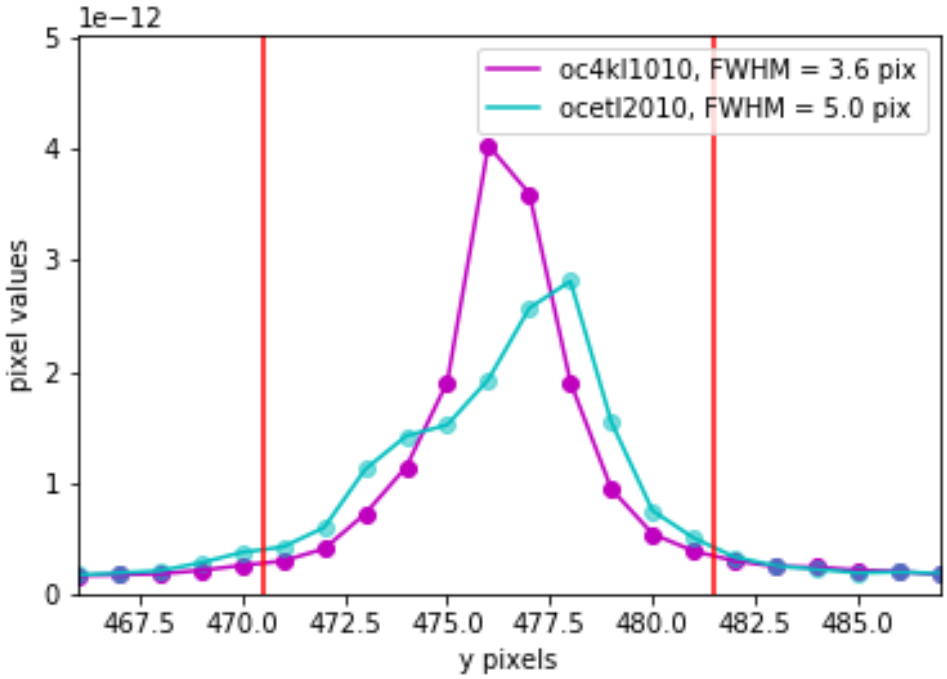

Figure 1.: Examples of the spatial profiles for the datasets with large and small FWHM. The red vertical lines show the 11-pixel extraction box for MAMA first-order gratings. These data were taken with the G140L grating at a central wavelength of 1425 Å.

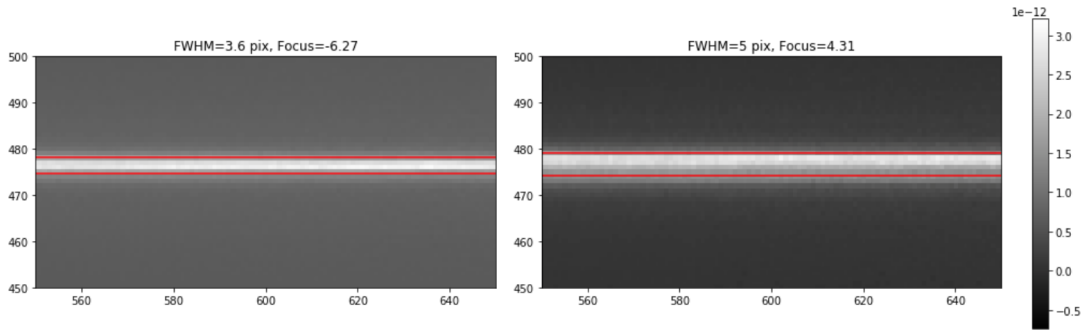

Figure 2.: Examples of what the spectrum may look like with different focus values. The left panel shows a spectrum with a FWHM of 3.6 pixels taken at a focus of -6.27 microns. The right panel shows a spectrum with a FWHM of 5 pixels taken at a focus of 4.31 microns. The red horizontal lines denote the boundaries of the FWHM. These data were taken with the G140L grating at a central wavelength of 1425 Å taken with the 52X2 aperture.

FWHM of 5 pixels and was taken when STIS was at a focus value of 4.31 microns. In fact, this dataset had one of the worst FWHM values in the set of data in which we first

noticed the unexpectedly large FWHMs. We derived these focus values from the HST focus model, which can be found at http://www.stsci.edu/hst/observatory/focus/FocusModel. Note that the model focus can be systematically off by ∼2-4 microns.

Figure 1 shows the spatial profiles of the same two datasets. Again, we see that the dataset with the negative focus value (oc4kl1010) has a much more compact spatial profile with a high peak. The other dataset however, is wider and is even asymmetrical and skewed.

2.2 Echelle Flux Anomalies

This document focuses on the first-order gratings, but complementary studies of the effect of focus on the echelle modes have been done as well. Since Servicing Mission 4 (SM4), many echelle observations of the standard star BD+284211 for the Time-Dependent Sensitivity (TDS) monitor have contained low throughputs. These echelle flux anomalies were previously documented by Bostroem, et al 2012 and were followed up by Debes, et al., (2018). The anomalous fluxes were found to be lower than expected by 5-10%, compared to reference observations, with the E140H/1416 and E230M/1978 settings most affected.

Spatial profiles of E140H/1416 and E230M/1978 TDS observations were visually inspected for asymmetries. Vertical slices from the central columns of FLT images were compared to corresponding reference observations, as shown in Figures 3 and 4. The anomalous flux observations had asymmetric profiles and lower count levels. These asymmetries are similar qualitatively to the asymmetries found for the first-order spectra discussed in Section 1, and illustrated in Figure 1. The echelle asymmetrical profiles could result in the Y-position centroids being slightly skewed in some observations. It was found that the average Y positional offsets compared to reference positions in the PHOTTAB reference files of the anomalous observations were generally larger or more positive than normal observations.

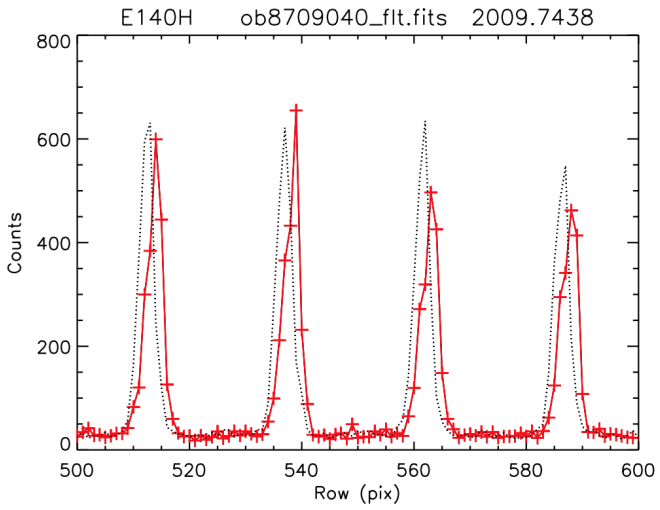

Figure 3.: Vertical slices from the centers of E140H FLT images. Plotted in red are the spatial profiles of anomalous observations. The dotted lines are the spatial profiles of the corresponding reference observations.

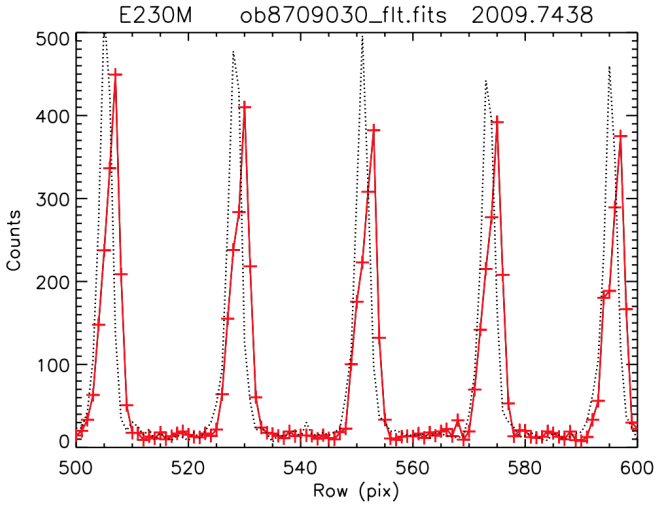

Figure 4.: Same caption as Figure 3 except for E230M.

The role of observatory focus on echelle flux anomaly occurrence was investigated by examining the behavior of the HST focus model, or orbital breathing, over the two-orbit TDS visits. Generally, it was found that anomalous observations occurred with the conditions of a positive focus value and during the steep declines in the focus model. Figure 5 demonstrates the focus changes due to breathing of a typical visit, where five observations are obtained over two orbits. Figure 6 includes a similar visit, but with

three echelle modes impacted by flux anomalies. The focus model values are positive in the anomalous observations and sample portions of the breathing curve where the focus value changes rapidly. These findings are in agreement with work by Proffitt, et al., (2017) that shows that STISs best focus tends to occur at negative focus model values. However, a few caveats need to be considered for any interpretations inferred using focus model values: 1. the focus model has intrinsic uncertainties and is not necessarily predictive of when a flux anomaly will occur, and 2. the focus model has not been updated recently by the Telescopes Branch and may not fully account for secular trends in the past 2-3 years. Thus, while the relative focus behavior is likely reproduced well by the focus model, the absolute focus value in microns of despace can be off by $\sim \pm 2$ microns (Proffitt, et al 2017).

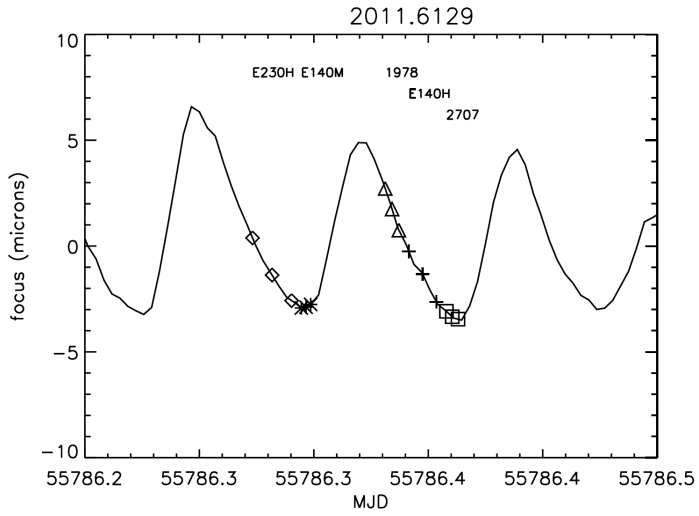

Figure 5.: HST model breathing curves for two visits. Points are plotted for the start, mid-point, and end of each observation. The points do not represent actual focus values measured but are used to guide the eye.

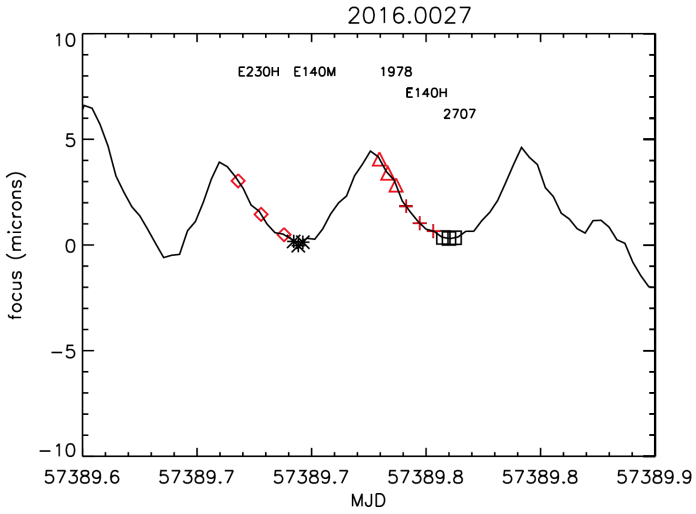

Figure 6.: HST model breathing curves for two visits. Points are plotted for the start, mid-point, and end of each observation. Anomalous observations are plotted in red. The points do not represent actual focus values measured but are used to guide the eye.

3. Calculating the Enclosed Energy Curves

Because there is evidence that the focus may be causing flux anomalies in the data from the first-order MAMA modes, we turned our attention to the EE tables used by the ETC. Given their uncertain origin, we wanted to know whether we could trace them back through documentation and whether they were still accurate. In this document, we will develop our own method of calculating the EE tables, determine how much the ETC has changed due to the focus, discuss the overall impacts on science data, and finish with a discussion of our work in the future.

3.1 Data Used to Generate EE Curves

To generate the EE curves, we used the data taken for the STIS MAMA Spectroscopic Sensitivity and Focus Monitor calibration program from Cycles 17 through 24 (PIDs 11860, 12414, 12775, 13145, 13548, 13994, 14429 and 14833). This program observes a spectrophotometric standard star in order to monitor the sensitivity of the MAMA detectors over time. This provided us with data for gratings G140L, G140M, G230L, and G230M at central wavelengths 1425, 1173 and 1567, 2376, and 2818, respectively.

The large amount of data allowed us to calculate the EE tables for these gratings as well as how the EE curves may have changed over time.

3.2 Method Used to Calculate EE Curves

In order to make exposure time calculations, the ETC uses a database file for each instrument, containing the EE tables of each grating. These tables include the EE values of various wavelengths across the wavelength range of that particular grating at various pixel heights, ranging from 1 to 1000 (taken to be where 100% of the source's flux is included). The table also includes from which document these EE tables were derived, oftentimes an Instrument Science Report (ISR), such as this one. In our case, all of the gratings for which we performed this investigation, pointed us to ISR 1998-01, suggesting these EE tables have not been updated since 1998. Upon further inspection of this ISR, there was no outline of the specific set of steps the author used to calculate the EE tables. Because of this, we created our own method and compared our results to those found by Bohlin, et al 1998 (see Section 4 for more information). Below is an outline of the steps we took:

- The **input** is a directory of files all taken with the same grating and central wavelength
- Determine the wavelengths to be used for each EE table.
  - Between 8 and 10 wavelengths, spanning the wavelength range of the grating.
  - Made sure not to include areas with obvious absorption or emission lines.
  - Two wavelength values just outside either end of the official wavelength range of the grating to account for any possible variation in the location of the spectrum.
- For each of the wavelengths across the range of the grating, and for each file,
  - background subtract using the average of a 30x30 pixel box at 300 pixels above and 300 pixels below the spectrum.
  - find the centroid of the spectrum by using a center of mass equation.
  - Calculate the EE by stepping out from the centroid location in both the positive and negative spatial directions and adding up all of the flux.
  - After the entire EE curve is calculated, find the EE value at a variety of extraction heights (1, 3, 5, 7, 9, 11, 21, ..., 600 pixels)
- Find the median of the calculated EE tables for a single wavelength in order to get a more accurate EE table across the many files used.
- For the end-wavelengths on the outskirts of the official wavelength range, fit a line across the wavelengths to get the EE values (see Figure 7)
- Save the results to a file.

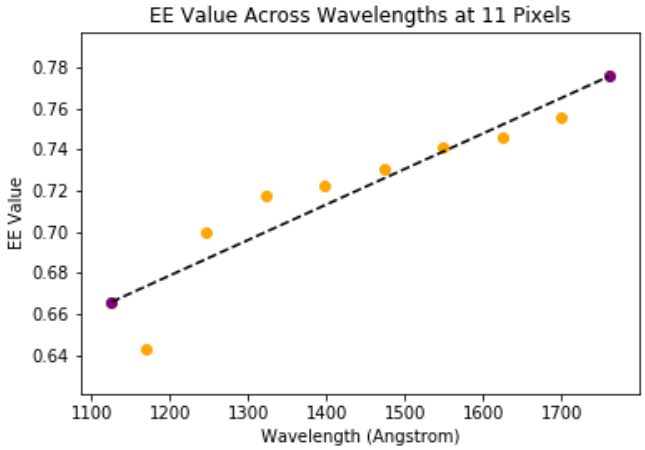

Figure 7.: A demonstration of how we calculated the EE values at the wavelengths just outside the official wavelength range. We fit a line to the inner wavelengths and evaluated the resulting equation at the outside wavelengths. The data points are discrepant from the fitted line by less than 7%.

Generally, this method worked well for our data. However, because the data we used for the G140M grating was taken at more than one central wavelength, and the wavelength ranges did not overlap, it was necessary to adopt a different approach.

The data for the G140M grating had central wavelengths at 1173 and 1567 Å, which cover 1145-1201 and 1540-1594, respectively. To account for the large gap in this data, we found data from an earlier version of the spectroscopic sensitivity monitor. This data was taken from PID 7657. We followed the same procedure outlined above for all three wavelength ranges and combined them all into one EE table. This way, the EE table spans the entire official wavelength range of the grating.

We adopted this method for G230M as well. In this case, the current MAMA sensitivity and focus monitor only provided data for one central wavelength, spanning only a very small portion of the overall wavelength range of the G230M grating. To fill out the analysis, we took data from PID 7657 and followed the same procedure established for G140M.

4. Results

The EE tables resulting from this analysis are discrepant from the EE tables currently in the ETC by, at most, $\sim$41% (Figure 8). Typically, we would only expect a discrepancy in the ETC by less than 10% due to regular errors in estimation. Because the discrepancy between the EE tables from this analysis and those in the ETC is so high, we can conclude that this is not from normal ETC estimation errors and can attributed to systematic errors in the ETC EE values themselves. This is most important for ETC

calculations that do not use the 11 pixel default extraction height for the MAMAs.

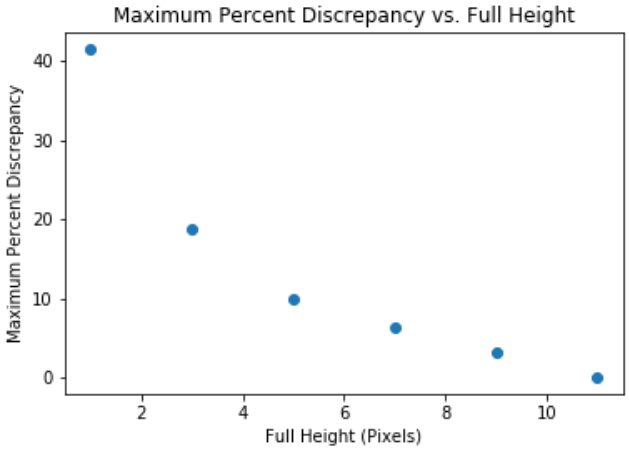

Figure 8.: The maximum percent discrepancy at various full heights.

For this analysis and interpreting our results, we took the results from Bohlin 1998 to be true, as this is the document listed as the pedigree in the EE tables and the results from this document were used in the PCTABs. But to verify that this assumption is reasonable, we plotted the EE tables resulting from this analysis over time and found that they have not changed appreciably since at least cycle 17. In Figure 9, we plotted the EE values for a single extraction height across wavelengths for each cycle since cycle 17. The panels show the EE values in the 1, 7, and 11 pixel extraction heights over time, from left to right. As we can see, EE values at 7 and 11 pixel extraction heights have changed only slightly in the past 8 cycles. This tells us that our default extraction height of 11 pixels from the first order MAMA modes is a large enough extraction height such that it will not be affected by positive focus. The EE values for the 1 pixel extraction height show much more variation, but no specific trend over time. This could be because the method described in section 3 does not take into account the subtleties of the 1 pixel extraction height. These subtleties are discussed in section 4.1.

To determine the accuracy of our results, we compared the results from this analysis to the results presented in ISR 1998-01, which are also the values in the PCTAB, as shown in Figures 10-13. We have already shown that the EE values have only slightly changed since cycle 17, but in fact, Figures 10-12 suggest that the EE values have not changed appreciably since 1998. Figure 13, on the other hand, had very limited data available to use in this analysis. One bad observation can throw off the analysis if the number of observations used was too low. For the L modes, we had almost 30 observations to analyze but with the M modes, we had less than 10. Because of this lack of data, we did not find an improvement in our most recent analysis. However, Figure 13 demonstrates that, like the other gratings, the EE values for the G230M grating in the ETC do not agree well with the values from the PCTAB. This warrants a redelivery of the PCTAB values to the ETC.

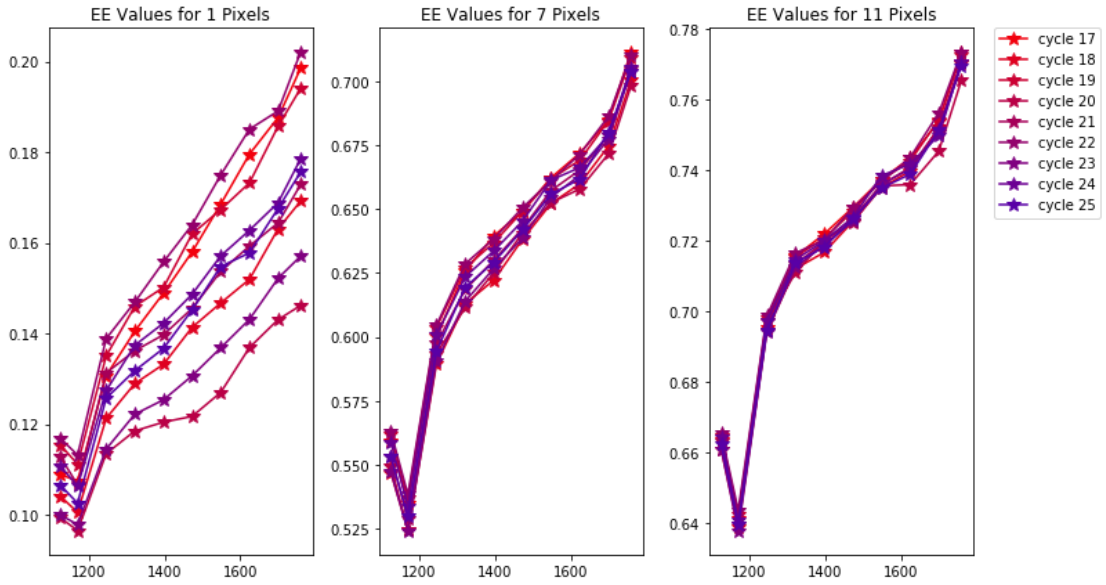

Figure 9.: The EE values over time appear to have changed only very slightly, although not in one particular direction. These changes are most seen in the EE values at 1 pixel. As the full height increases, the change in EE values over time becomes smaller and smaller.

Because the EE tables from the ETC are very discrepant from the PCTAB values, we can conclude that the EE tables in the ETC are the reason we are seeing discrepancies in the observed flux values. It is important to note that the 3-pixel aperture appears to deviate between the PCTAB and the results of this analysis. This is consistent with the slight variability seen from cycle-to-cycle for small extraction heights (see Figure 9).

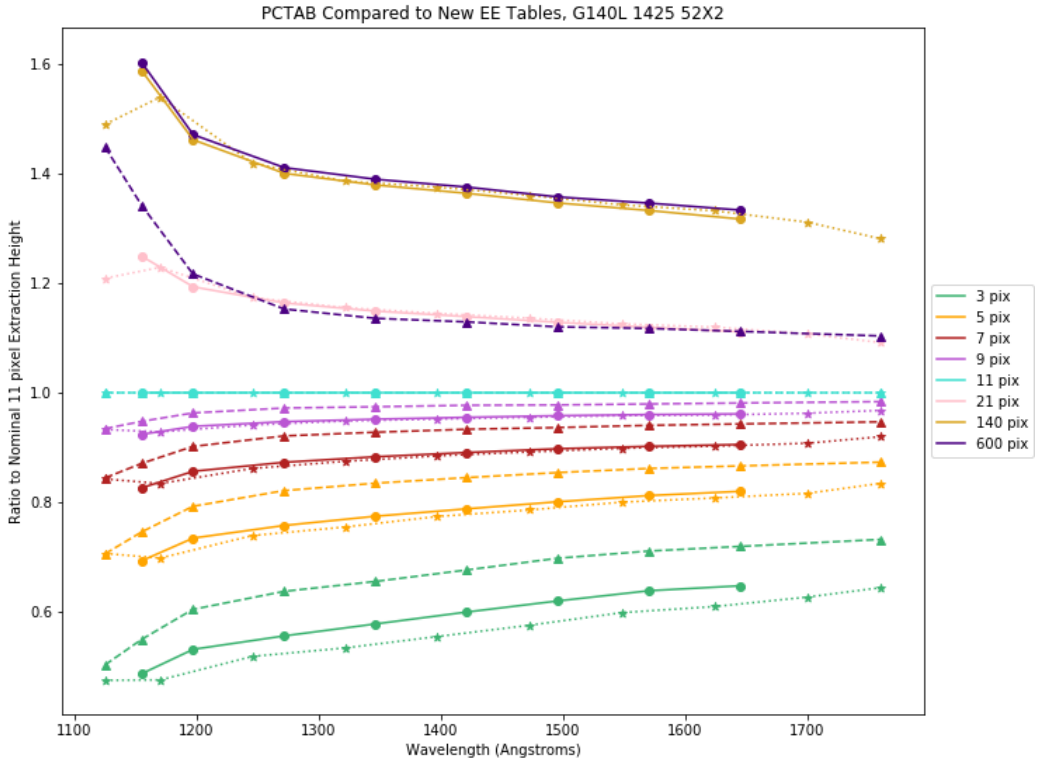

Figure 10.: The results with a grating of G140L and a central wavelength of 1425 Å. The values resulting from this analysis are plotted in dotted line with stars. Plotted in solid lines with circles, are the values from the PCTAB, which are the same as the resulting values from Bohlin, 1998. The values from the ETC are plotted in dashed lines with triangle-shaped points. The values used in the ETC do not agree well with the values from Bohlin, 1998. This could be due to poor bookkeeping about where the values in the ETC originated from.

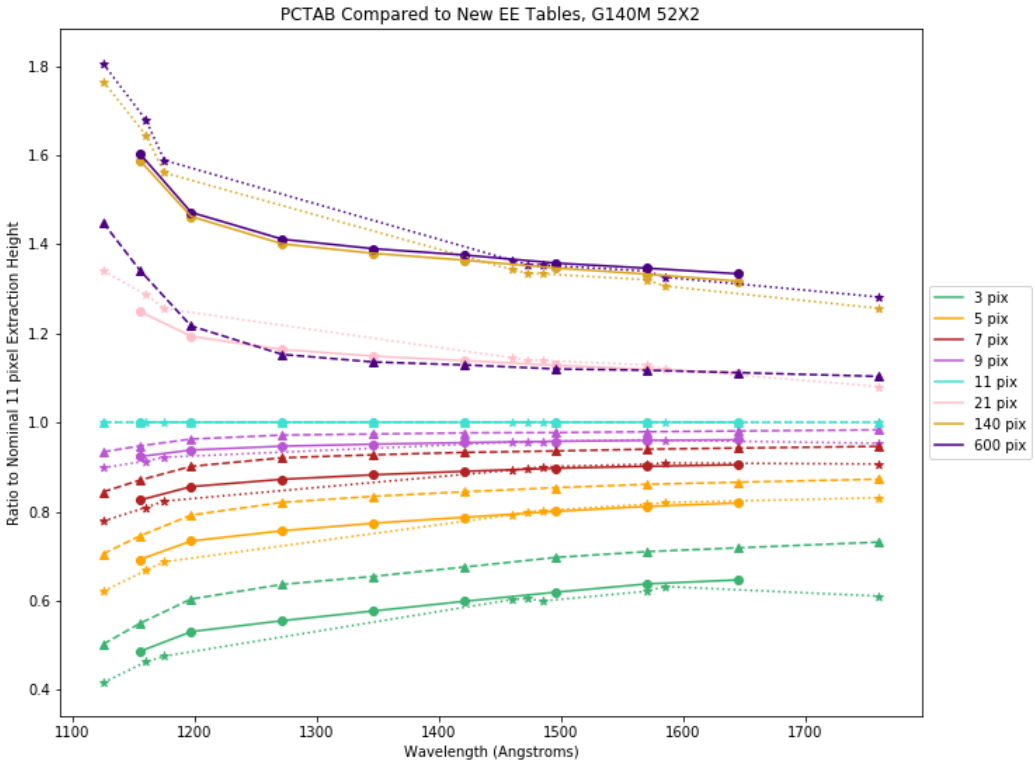

Figure 11.: See Figure 10 caption, except for G140M with central wavelengths 1173, 1470, and 1567 Åand with the 52X2 aperture.

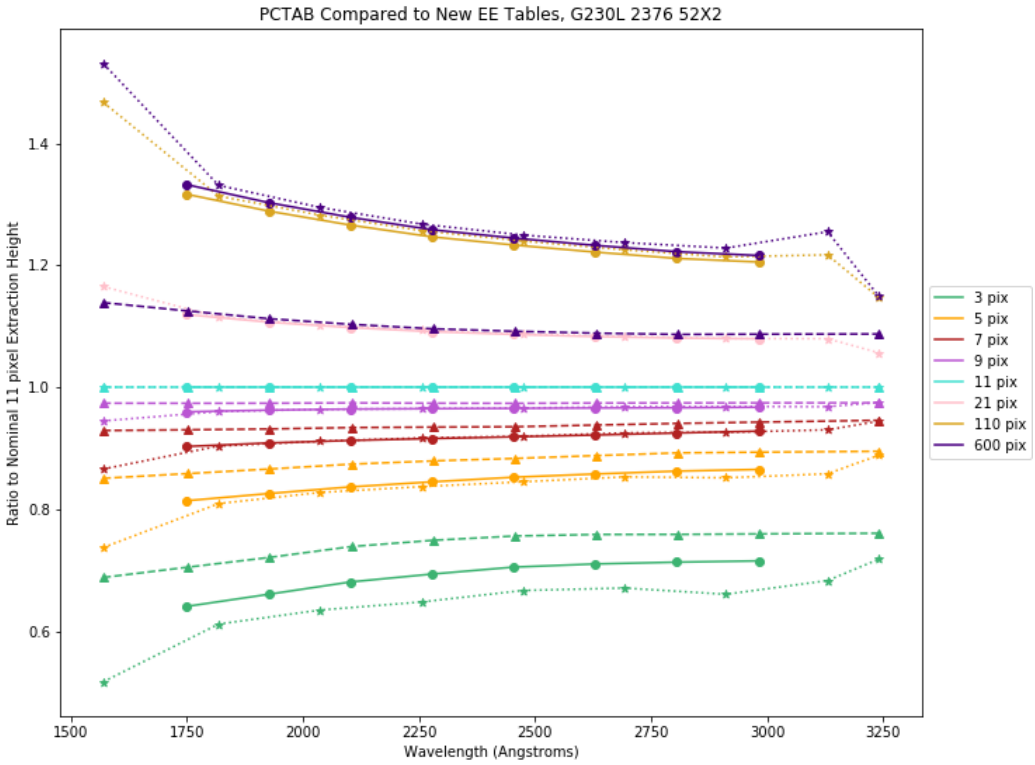

Figure 12.: See Figure 10 caption, except for G230L, at a central wavelength of 2376 Å, and aperture 52X2.

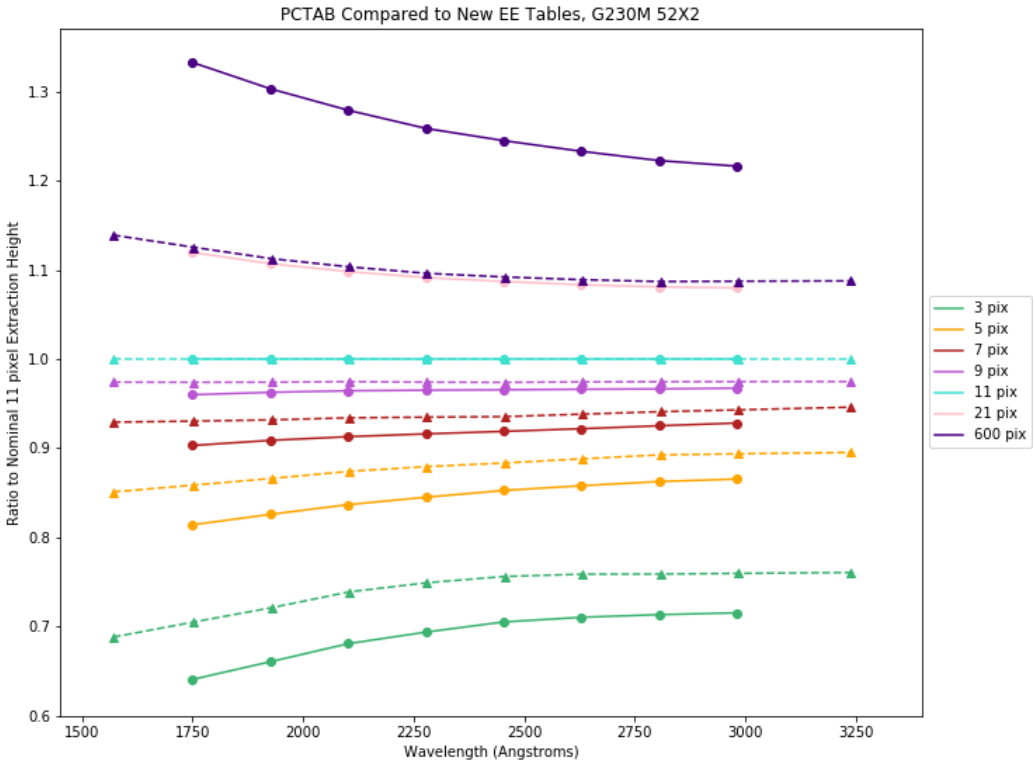

Figure 13.: This figure shows how discrepant the ETC values (dashed lines with triangles) are to the values calculated in 1998 and the PCTAB values (solid lines with circles). Because the ETC values were so discrepant from the PCTAB values, we will redeliver the PCTAB values to the ETC. These data were taken with G230M grating and the 52X2 aperture.

Finally, we compared our results to those found by Leitherer and Bohlin (1997). Similarly to their analysis, we set the background to be at 300 pixels out from the spectrum and assumed the flux to be 100% at 600 pixels. They found that the EE values for G140L were ∼70% of the total extracted flux at 11 pixels, and it jumps to ∼80% of the total extracted flux at 21 pixels (Leitherer and Bohlin, 1997). Table 1 agrees well with this finding and appear to only be off by no more than 7%. For G230L, Leitherer and Bohlin (1997) found that, at 11 pixels, the flux was between 73% and 81% and for 21 pixels, it was ∼10% higher. Table 3 were no more than 8% discrepant from this. Both of these comparisons show further that the EE values have not changed substantially throughout the history of STIS and they also confirm the results from the analysis discussed in this document.

4.1 1 Pixel Analysis

It is important to note that the analysis so far does not take into account whether the spectrum is centered on the pixel, which may cause the results for the 1 pixel full width to be incorrect. In order to rectify this, we also did a complementary analysis.

To better estimate the EE at 1 pixel full height, we plotted the pixel value in the pixel with the brightest flux, according to the EXTRLOCY header keyword divided by the net flux in the extraction box (11 pixels for the MAMAs). Figures 14-16 show how the EE ratios from this analysis compare to the EE ratios from the EE table in the ETC as well as actual observations. Ideally, the EE ratios should align well with the top envelope of the blue and green lines. The black line, from the ETC, shows that right now, the ETC is overestimating the flux in the brightest pixel at lower wavelengths and underestimating the flux at higher wavelengths. The red line, denoting the results from this analysis, shows a large improvement.

This secondary analysis was important to the final EE tables that we will inevitably include into the ETC because the 1 pixel values are what the ETC uses to estimate the brightest pixel in a possible observation. This is extremely important in protecting the MAMA detectors from bright objects that could damage them. To do this, we took the EE tables resulting from the analysis in section 3.2 and applied a correction so that it matches the upper envelope seen in Figures 14-16. We wanted the 1 pixel value in the EE tables to match up to the brightest scenario so that the ETC does not underestimate the brightest pixel. The results of this 1 pixel analysis were used as the 1 pixel value for the final EE tables detailed in Tables 1-3.

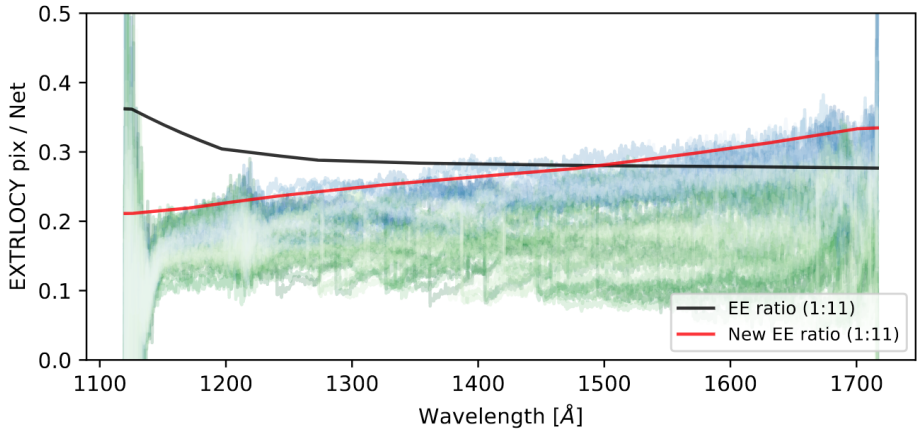

Figure 14.: The blue and green lines show the brightest pixel value divided by the net count for many observations with the G140L grating. The blue lines show the pixel value in the brightest pixel and the green lines denote the pixel values in the pixels neighboring the brightest pixel. The black line shows the EE ratio of 1 to 11 pixels, according to the ETC and the red line shows the ratio of 1 to 11 pixels, according to the analysis presented in this document.

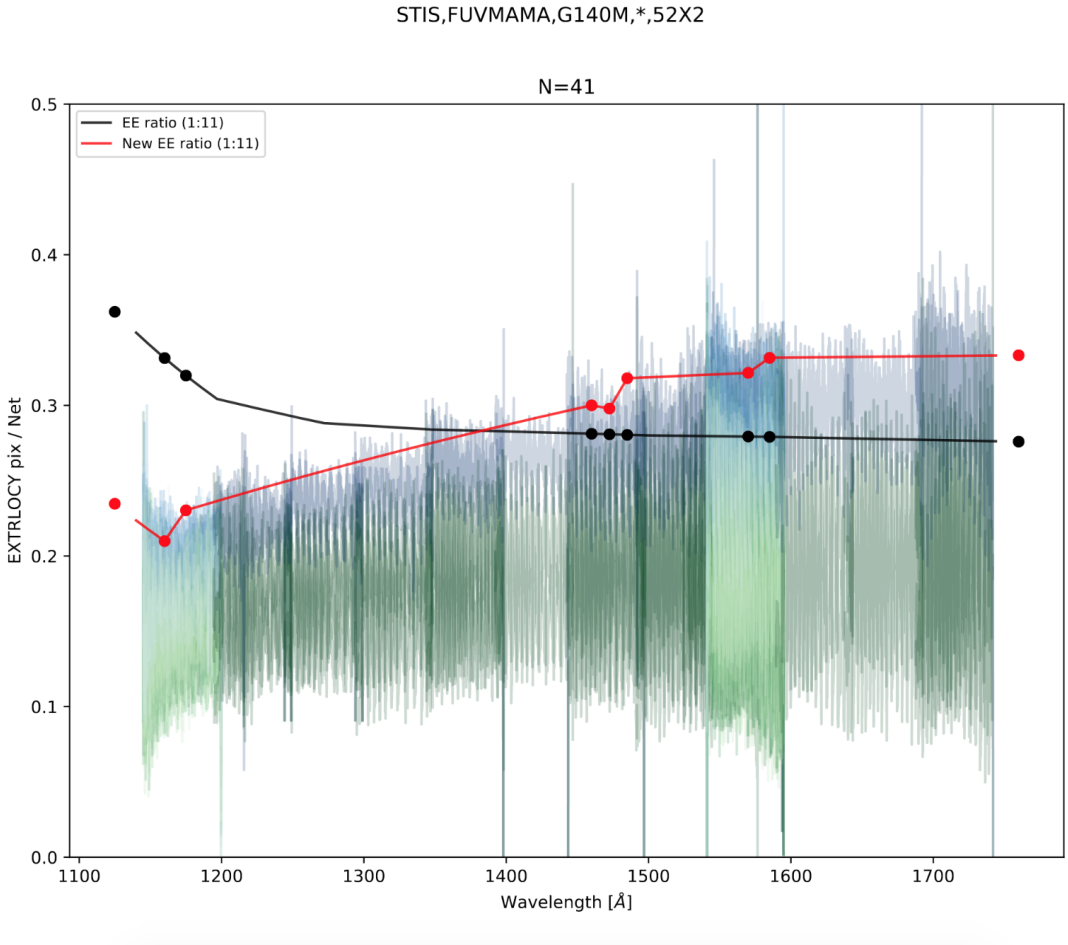

Figure 15.: Same caption as Figure 14 except with G140M. This figure looks a bit different because there are many central wavelengths across the G140M grating. We only sampled using three central wavelengths (1173, 1470, 1567 Å).

The final EE tables from this analysis are given in Tables 1-3.

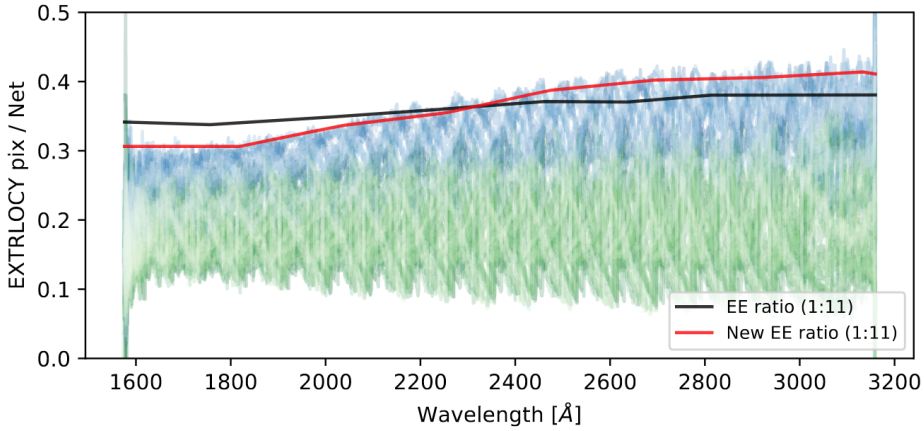

Figure 16.: Same caption as Figure 14 except with G230L.

Wavelength	1	3	5	7	9	11	21	41	61	81	141	600
1125.0	0.14	0.31	0.47	0.56	0.62	0.66	0.79	0.92	0.96	0.97	0.99	1.
1170.0	0.14	0.30	0.45	0.53	0.59	0.64	0.77	0.91	0.95	0.97	0.98	1.
1245.71	0.17	0.36	0.51	0.60	0.65	0.70	0.81	0.92	0.96	0.97	0.99	1.
1321.43	0.18	0.38	0.54	0.62	0.68	0.71	0.82	0.93	0.96	0.97	0.99	1.
1397.14	0.19	0.40	0.56	0.64	0.68	0.72	0.82	0.92	0.96	0.97	0.99	1.
1472.86	0.20	0.42	0.57	0.65	0.69	0.73	0.82	0.92	0.96	0.97	0.99	1.
1548.57	0.22	0.44	0.59	0.66	0.70	0.74	0.82	0.92	0.96	0.97	0.99	1.
1624.29	0.23	0.45	0.60	0.67	0.71	0.74	0.82	0.92	0.96	0.97	0.98	1.
1700.0	0.25	0.47	0.61	0.68	0.72	0.75	0.82	0.92	0.95	0.97	0.98	1.
1760.0	0.26	0.50	0.64	0.71	0.75	0.77	0.83	0.92	0.96	0.97	0.99	1.

Table 1.: The EE table that we computed for the G140L grating using the method described in Section 3.2. The first and last wavelengths (1125 and 1760 Å) are slightly outside the official wavelength range of G140L.

Wavelength	1	3	5	7	9	11	21	41	61	81	141	600
1125.0	0.089	0.23	0.34	0.43	0.50	0.55	0.73	0.89	0.94	0.96	0.98	1.
1160.0	0.13	0.28	0.40	0.48	0.54	0.59	0.75	0.90	0.94	0.96	0.98	1.
1175.0	0.13	0.30	0.43	0.52	0.58	0.63	0.78	0.91	0.95	0.96	0.98	1.
1460.0	0.22	0.44	0.58	0.66	0.70	0.73	0.83	0.93	0.96	0.97	0.98	1.
1485.0	0.24	0.44	0.59	0.67	0.71	0.74	0.83	0.93	0.96	0.97	0.99	1.
1570.0	0.24	0.46	0.61	0.68	0.72	0.75	0.84	0.93	0.96	0.97	0.98	1.
1585.0	0.25	0.48	0.62	0.69	0.72	0.75	0.84	0.93	0.96	0.97	0.98	1.
1760.0	0.26	0.48	0.65	0.71	0.74	0.78	0.84	0.93	0.97	0.97	0.98	1.

Table 2.: The EE table that we computed for the G140M grating using the method described in Section 3.2. The first and last wavelengths (1570 and 3240 Å) are slightly outside the official wavelength range of G140M.

Wavelength	1	3	5	7	9	11	21	41	61	81	141	600
1570.0	0.20	0.34	0.48	0.57	0.62	0.65	0.75	0.87	0.92	0.94	0.96	1.
1818.6	0.23	0.46	0.61	0.68	0.72	0.75	0.83	0.92	0.96	0.97	0.99	1.
2037.1	0.26	0.49	0.64	0.70	0.74	0.77	0.85	0.93	0.96	0.98	0.99	1.
2255.7	0.28	0.51	0.66	0.72	0.76	0.79	0.86	0.93	0.96	0.98	0.99	1.
2474.3	0.31	0.53	0.68	0.74	0.77	0.80	0.87	0.93	0.96	0.98	0.99	1.
2692.9	0.33	0.54	0.69	0.75	0.78	0.81	0.87	0.93	0.96	0.98	0.99	1.
2911.4	0.33	0.54	0.69	0.75	0.79	0.81	0.87	0.93	0.96	0.97	0.99	1.
3130.0	0.33	0.54	0.68	0.74	0.77	0.80	0.86	0.91	0.93	0.95	0.97	1.
3240.0	0.35	0.62	0.77	0.82	0.85	0.87	0.92	0.95	0.97	0.99	0.99	1.

Table 3.: The EE table that we computed for the G230L grating using the method described in Section 3.2. The first and last wavelengths (1570 and 3240 Å) are slightly outside the official wavelength range of G230L.

5. Conclusions and Future Work

After calculating new EE tables for the first-order MAMA modes, we found that for three of the four modes, the EE tables currently used by the ETC are likely inaccurate. In fact, the discrepancy between the current EE tables and those resulting from this analysis are discrepant by up to 41%. where we would typically expect discrepancies of less than 10%. Due to the long interval over which these EE tables have been used, the STIS team verified that there has been no significant evolution of the EE values at 7 and 11 pixels since cycle 17 and, in fact, since 1998. Once delivered and implemented into the ETC, these EE tables will provide more accurate estimates of STIS performance and, as a result, help improve estimates for bright object protection.

However, the focus may continue to drift in a positive direction, away from STIS best focus. The fact that there has been little change in the EE values despite the degrading focus, tells us that the extraction size of 11 pixels used for the MAMAs is still an appropriate size. This way, it is overwhelmed by neither background noise nor flux variations due to focus.

5.1 Notes to the User Community

The default extraction box height for echelle observations in the CalSTIS pipeline is 7 pixels. If asymmetric profiles are noticed in a given observation, it may be possible to recover a small percentage of the flux by expanding the extraction box height to 9 or 11 pixels. However, the efficacy of this suggestion has not been established and may not be suitable for low SNR observations.

In terms of the first order modes, if the data in question exhibits asymmetric profiles, it is likely due to positive focus values at the time of the observation. To check this, the focus model values can be found at http://www.stsci.edu/hst/observatory/focus/FocusModel. Positive focus values can impact the flux levels, especially for small slits ($\sim$ .2"). If the science requires repeatable flux accuracy in the UV, one may consider using a wider slit. Similarly, in the case of long slits, flux can be recovered, but not necessarily for narrow slit sizes.

Before observation, when using the ETC to check exposure time or signal-to-noise, the default slits are okay to use for the ETC, but if a non-standard extraction box is used, there may be some discrepancies in predicted flux and actual flux. This is something that the STIS team is currently working on. It is important to know that larger extraction boxes may have higher background noise. When deciding whether to use a different slit width, balancing those two aspects will be necessary.

5.2 Future Work

In order to deliver these new EE tables to the ETC, we will run extensive tests on them to ensure that they are producing the expected exposure times and signal-to-noise ratios,

given various input parameters.

We would also like to perform similar analysis on the rest of the MAMA gratings. For this analysis, we used only the data included in the Spectroscopic Sensitivity and Focus Monitors since SM4, which only includes data for specific modes. In order to investigate the EE tables for other modes not included in the Spectroscopic Sensitivity and Focus Monitor, we will need to use science data of a point source.

Finally, we would like to cross-correlate these with the Sharpness tables, which are used to calculate signal-to-noise levels in photometric data. The sharpness tables are derived from the EE tables, so we would like to re-derive them in order to make them as accurate as possible.

Acknowledgements

We thank the STIS team for insightful discussions about the performance of the CCD and for taking the time to edit this document.

Change History for STIS ISR 2018-06

Version 1: November 7, 2018- Original Document

References

Bohlin, R. 1998, ”Diffuse Source Absolute Sensitivity and Point Source Relative Sensitivity as a Function of Extraction Slit Height for STIS First-Order Modes.” STIS ISR 1998-01.

Bostroem, K.A., Aloisi, A., Bohlin, R., Hodge, P., Proffitt, C. 2012, ”Post-SM4 Sensitivity Calibration of the STIS Echelle Modes.” STIS ISR 2012-01.

Debes, J., Lockwood, S.A., Monroe, T.R., Proffitt, C., Riley, A. 2018. ”Summary of STIS Functional Mini-Sabbaticals: Fiscal Year 2017.” STIS TIR 2018-01.

Leitherer, C., Bohlin, R. 1997. ”Extraction Slits for First Order STIS Spectra.” STIS ISR 1997-13.

Proffitt, C.R., Monroe, T., Dressel, L. 2017, ”Status of the STIS Instrument Focus.” STIS ISR 2017-01.

Appendix A

Wavelength	1	3	5	7	9	11	1000
1125.00	0.25	0.3470	0.4871	0.5829	0.6450	0.6904	1.
1155.00	0.25	0.4093	0.5556	0.6489	0.7061	0.7452	1.
1196.83	0.25	0.4962	0.6510	0.7409	0.7912	0.8217	1.
1271.52	0.25	0.5524	0.7121	0.7988	0.8430	0.8674	1.
1346.21	0.25	0.5766	0.7347	0.8167	0.8577	0.8804	1.
1420.91	0.25	0.5985	0.7480	0.8262	0.8650	0.8855	1.
1495.60	0.25	0.6225	0.7622	0.8357	0.8725	0.8926	1.
1570.29	0.25	0.6359	0.7710	0.8415	0.8765	0.8950	1.
1644.99	0.25	0.6466	0.7789	0.8479	0.8823	0.8993	1.
1760.00	0.25	0.6630	0.7910	0.8577	0.8912	0.9061	1.

Table 4.: The EE table for the G140L grating used currently in the ETC.

Wavelength	1	3	5	7	9	11	1000
1125.00	0.25	0.3470	0.4871	0.5829	0.6450	0.6904	1.
1155.00	0.25	0.4093	0.5556	0.6489	0.7061	0.7452	1.
1196.83	0.25	0.4962	0.6510	0.7409	0.7912	0.8217	1.
1271.52	0.25	0.5524	0.7121	0.7988	0.8430	0.8674	1.
1346.21	0.25	0.5766	0.7347	0.8167	0.8577	0.8804	1.
1420.91	0.25	0.5985	0.7480	0.8262	0.8650	0.8855	1.
1495.60	0.25	0.6225	0.7622	0.8357	0.8725	0.8926	1.
1570.29	0.25	0.6359	0.7710	0.8415	0.8765	0.8950	1.
1644.99	0.25	0.6466	0.7789	0.8479	0.8823	0.8993	1.
1760.00	0.25	0.6630	0.7910	0.8577	0.8912	0.9061	1.

Table 5.: The EE table for the G140M grating used currently in the ETC.

Wavelength	1	3	5	7	9	11	1000
1570.00	0.30	0.6042	0.7470	0.8158	0.8552	0.8779	1.
1752.54	0.30	0.6266	0.7630	0.8268	0.8655	0.8886	1.
1928.50	0.31	0.6482	0.7785	0.8375	0.8755	0.8988	1.
2104.46	0.32	0.6697	0.7922	0.8466	0.8833	0.9063	1.
2280.41	0.33	0.6835	0.8023	0.8529	0.8887	0.9123	1.
2456.37	0.34	0.6925	0.8090	0.8566	0.8918	0.9157	1.
2632.33	0.34	0.6968	0.8156	0.8616	0.8948	0.9183	1.
2808.29	0.35	0.6982	0.8212	0.8657	0.8966	0.9200	1.
2984.25	0.35	0.6987	0.8220	0.8673	0.8964	0.9197	1.
3240.00	0.35	0.6994	0.8231	0.8698	0.8962	0.9194	1.

Table 6.: The EE table for the G230L grating used currently in the ETC.

Wavelength	1	3	5	7	9	11	1000
1570.00	0.30	0.6042	0.7470	0.8158	0.8552	0.8779	1.
1752.54	0.30	0.6266	0.7630	0.8268	0.8655	0.8886	1.
1928.50	0.31	0.6482	0.7785	0.8375	0.8755	0.8988	1.
2104.46	0.32	0.6697	0.7922	0.8466	0.8833	0.9063	1.
2280.41	0.33	0.6835	0.8023	0.8529	0.8887	0.9123	1.
2456.37	0.34	0.6925	0.8090	0.8566	0.8918	0.9157	1.
2632.33	0.34	0.6968	0.8156	0.8616	0.8948	0.9183	1.
2808.29	0.35	0.6982	0.8212	0.8657	0.8966	0.9200	1.
2984.25	0.35	0.6987	0.8220	0.8673	0.8964	0.9197	1.
3240.00	0.35	0.6994	0.8231	0.8698	0.8962	0.9194	1.

Table 7.: The EE table for the G230M grating used currently in the ETC.